Progress In Electromagnetics Research B, Vol. 102, 19–35, 2023

Assessment of Human Exposure to High Frequency Fields Generated by Wireless Transmitters: A Simplified Analytical Model

Petra Rašić*, Zoran Blažević, and Dragan Poljak

Abstract—This work examines the effects of high frequency radio transmission on the human body. A magnetic point source is used to generate a signal that is transmitted through the human body at a specified distance. The study was conducted to evaluate the health effects of exposure to high frequency radiation, in relation to current density, induced electric field and specific absorption rate at frequencies of 6.78 MHz and 13.56 MHz. The results for both an equivalent cylinder and a realistic human body model were compared. The analytical method presumes a sinusoidal current distribution along the cylinder and introduces the approximations of field integrals. The numerical simulations by the commercial software FEKO confirmed the analytical results depicted in the paper. The study shows that maximum differences between the results of the proposed analytical model and human model (regardless being realistic or cylinder) are less than 10%. This is convenient because analytical methods can ensure fast estimations of the exposure standard limitations.

1. INTRODUCTION

The surge in electricity use over the past half century demonstrates the vital role it plays in modern society. Most of these contemporary devices that people use generate high intensity electromagnetic fields that could be hazardous to human health. People worry about the possible harm that electromagnetic fields might cause to their health. By interfering with endogenous physiological processes, both induced and contact currents might disturb biological functioning. This might result in neurological, muscular, and/or neurovascular activation. Its condition might induce muscular spasms, hearing and vision perceptions, ocular coordination issues, disorientation, metal flavour, and a surge in mental fogginess [1–3]. Electrostimulation of electrosensitive tissues predominates when they are exposed to electromagnetic fields (EMFs) with frequencies less than 100 kHz; however, this phenomenon could also happen when the human body is exposed to EMFs with frequencies ranging from 5 to 20 MHz [1, 4]. Those currents could also generate heating consequences, a rise in the heating of organs within or on the body's surface, which could result in thermal injury. When the human body is exposed to EMF frequencies exceeding 100 kHz, thermal consequences might occur. Thermal effects become the major phenomena above 10 GHz [1, 5, 6]. Due to the greater conductivity of bone tissue than muscle tissue, flowing currents reach the maximum intensity in regions where the cross-section of the body tightens (e.g., ankle, knee, wrist, and head). Those tend to be the most sensitive areas, where the effects of current flow, such as resistant warming of tissue, manifest themselves first. As a result, the key concern is determining the strength of the current that flows in the legs, particularly when the worker touches components near the source of the EMF (hand current) [7, 8]. The impacts indicated above could induce disruptions inside the body's functioning, which may put at risk the security of executing work activities and, in the case of prolonged exposure, might produce possible health issues [9–11].

Received 20 April 2023, Accepted 8 July 2023, Scheduled 3 August 2023

* Corresponding author: Petra Rašić (prasic@fesb.hr).

The authors are with the Faculty of Electrical Engineering, Mechanical Engineering and Naval Architecture, University of Split, Split 21000, Croatia.

Realistic human models are highly accurate, while simplified models are faster to estimate the radiation exposure. In order to calculate realistic human body models, it is needed to apply full wave models which requires numerical calculation techniques like Finite Element Method (FEM) [12–14], Boundary Element Method (BEM) [15–19], or robust methods like Finite Difference Method (FDTD). These techniques are applied to estimate the exposure of individual body parts or entire body. These calculations can be time-consuming, and a complicated method implementation is often needed [20–24]. Studies have been conducted to determine the exposure levels that are safe in relation to basic restrictions [25–30]. Simulations of the human body are performed to help understand how the body's wireless power transfer (WPT) antenna works. This information is used to improve the design of WPT antennas. In [27], the authors discuss the exposure of humans to WPT systems and present evaluations of a realistic human model which was exposed to high frequency (HF) radiation at 6.78 MHz and at 100 kHz [28–32]. A dielectric box, or model of a human, was used to study how it affects the performance of WPT systems. This was investigated in the study given in [33] where a large rectangular loop was used as a transmitting antenna.

This paper investigates the feasibility of an analytical modelling approach by the antenna theory for basic human exposure analysis using simplified calculations. The first step is using the human body model that is similar to the one in [10, 11]. The model is based on Pocklington-type equations, which can be used to calculate the effects of antennas on a person. Differences between the results of the analysis and numerical modelling are explored and discussed. The considered scenario of WPT environment consists of a human and an antenna. The antenna is a magnetic point source transmitting at two different frequencies, $f = 6.78\,\text{MHz}$ and $f = 13.56\,\text{MHz}$. These frequencies fall within the range of frequencies allocated for Industrial, Scientific and Medical (ISM) purposes. Besides the reasons of selecting standard ISM frequencies for WPT purposes, we want to address some parameters usually occurring in International Commission on Non-Ionizing Radiation Protection (ICNIRP) recommendations. "Old" ICNIRP recommendations refer to the frequencies below 10 MHz (which observes the induced current density) [33] and above 10 MHz (which observes SAR). On the other hand, "new" ICNIRP recommendations refer to the frequencies below 6 MHz (which observes the induced electric field) and above 6 MHz (which observes SAR) [1]. The proposed cylinder model and the realistic model were used to compare currents, induced electric fields, and specific absorption rate (SAR) in the body caused by the external field irradiated by a radio frequency (RF) transmitting antenna. The results of this comparison were referenced to international protection exposure standard given in [1, 32, 33]. This simplified analytical model based on the solution of Pocklington-integral equation derived in this paper is the first of its kind for WPT use in near field at ISM bandwidth, where induced current density, induced electric field, and SAR are analysed as a continuation of our previous investigation presented in [34].

The organization of paper is as follows. Section 2 presents an analytical formulation of the human body exposure to the near field of HF transmitting antenna used for WPT. Full wave model calculation by FEKO is discussed in Section 3, while observations are depicted and discussed in Section 4. The paper is concluded in Section 5.

2. ANALYTICAL FORMULATION

Figure 1 illustrates the propagation geometry in relation to a human body modelled as a thin cylinder exposed to specified RF fields. It is supposed that humans are in free space with their limbs firmly fastened to their bodies. The human of height $L = 1.8\,\text{m}$ and torso diameter $2a = 33.34\,\text{cm}$ is modelled as an equivalent cylinder with corresponding tissue electrical properties [35]. According to the model assumption, the cylinder's height L and width $2a$ are equivalent to the height and width of a typical person. The homogeneous, isotropic lossy material that makes up a realistic human is modelled as being similar to [10]. The cylinder body model has a total volume of $0.046\,\text{m}^3$. The realistic, full body model has a volume of $0.055\,\text{m}^3$.

At frequencies of 6.78 MHz and 13.56 MHz, the relative permittivity of the human body is assumed to be $\varepsilon_r = 92$, the tissue density assumed to be $\rho = 1000\,\text{kgm}^{-3}$, and the specific conductivity assumed to be $\sigma = 0.419\,\text{Sm}^{-1}$ [35]. As a result, the cylinder's complex permittivity is given by $\varepsilon_C = \varepsilon_{Cr}\varepsilon_0$, $\varepsilon_{Cr} = 92 - j1112$, ($\varepsilon_0$ is the permittivity of vacuum), where the imaginary part is significantly larger

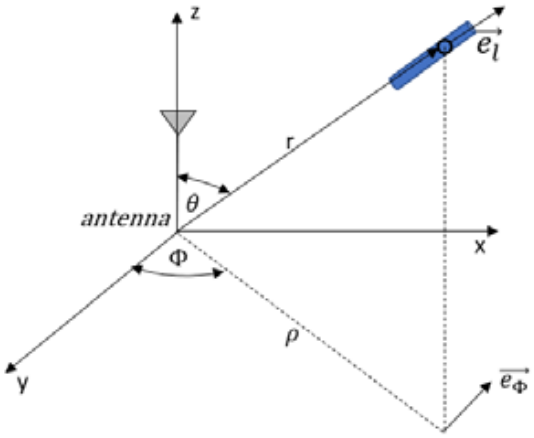

Figure 1. TE_{10} mode for near field modeling.

than the real part. This means that the body acts as a lossy conductor at the frequencies in question. It is assumed that the permeability equals the one of free space ($\mu = \mu_0$).

The skin depth can be calculated as:

$$\delta_{\text{skin}} = \sqrt{\frac{2}{\omega\mu\sigma}} \tag{1}$$

According to Eq. (1), the skin depth counts 29.88 cm for the frequency $f = 6.78$ MHz and 21.11 cm for the frequency $f = 13.56$ MHz, indicating that the currents penetrate the entire cylinder's cross-section. The surface impedance is given by [10]:

$$Z_s(\zeta) = \frac{Z}{2\pi a}\frac{J_0(\gamma_w, \zeta)}{J_1(\gamma_w, a)} \tag{2}$$

where J_0 and J_1 are the zeroth and first order Bessel functions, respectively, and $0 \leq \zeta \leq a$. Z and γ_w are expressed as:

$$Z = \sqrt{\frac{j\omega\mu}{\sigma + j\omega\varepsilon}} \tag{3}$$

$$\gamma_w = \sqrt{j\omega\mu(\sigma + j\omega\varepsilon)} \tag{4}$$

where $\varepsilon = \varepsilon_r\varepsilon_0$ is the permittivity.

2.1. Electric Field

The electrically short magnetic dipole of radiation efficiency η_{rad}, fed by power P_G provided by a matched generator, radiates electric field transversally electric TE_{10} mode at a distance r which is given by [26]:

$$\vec{E} = -j\beta\sqrt{\frac{3PZ_0}{4\pi}}\left[\frac{1}{j\beta r} + \frac{1}{(j\beta r)^2}\right]\sin\theta e^{-j\beta r}\overrightarrow{e_\phi} \tag{5}$$

where $Z_0 = 120\pi\Omega$ is the free-space impedance, θ the angle of elevation, and $\beta = 2\pi/\lambda$ the propagation constant, whereas P is the power radiated by the dipole:

$$P = \eta_{\text{rad}}P_G \tag{6}$$

The antenna's axis coincides to the z-axis of the referent coordinate system. The cylinder's axis can be typically found in the following directions:

$$\overrightarrow{e_l} = \cos\phi_C\sin\theta_C\overrightarrow{e_x} + \sin\phi_C\sin\theta_C\overrightarrow{e_y} + \cos\theta_C\overrightarrow{e_z} \tag{7}$$

With an assumption that the observed segment of the cylinder is located at $l = l(r, \phi, \theta)$, the incident field at the axis of the cylinder is calculated as:

$$E_l(l) = E(r, \phi, \theta)\, \overrightarrow{e_\phi} \cdot \overrightarrow{e_l} \tag{8}$$

i.e., by inserting Eq. (7) into Eq. (8):

$$E_l = -j\beta\sqrt{\frac{3PZ_0}{4\pi}}\left[\frac{1}{j\beta r} + \frac{1}{(j\beta r)^2}\right](\sin\phi_C \sin\theta_C \cos\phi - \cos\phi_C \sin\theta_C \sin\phi)\sin\theta e^{-j\beta r} \tag{9}$$

2.2. Current Density and SAR

The Pocklington integro-differential equation describes the current distribution on a thin wire of finite conductivity (used for example in human exposure scenario or in electromagnetic compatibility to calculate the effects of nearby thin-wire objects on WPT system), and it is given by [10]:

$$\int_0^L \left(\frac{\partial^2}{\partial l^2} + \beta^2\right) I(l')\, g(l, l')\, dl' - j4\pi\frac{\beta}{Z_0} Z_S(l) I(l) = -j4\pi\frac{\beta}{Z_0} E_z(l) \tag{10}$$

where $I(l)$ is the current distribution on the wire, and $g(l, l')$ is the Green function:

$$g(l, l') = \frac{e^{-j\beta\sqrt{a^2 + (l-l')^2}}}{\sqrt{a^2 + (l-l')^2}} \tag{11}$$

The characteristic integral from the Pocklington equation should be written as:

$$\int_0^L I(l')\, g(l, l')\, \mathrm{d}l' = I(l)\int_0^L g(l, l')\, \mathrm{d}z' + \int_0^L \left[I(l') - I(l)\right] g(l, l')\, \mathrm{d}l' \tag{12}$$

Using the assumption that the current varies slowly, i.e., $I(l) \approx I(l')$ [29], the first term on the right roughly approximates the integral on the left, and thus the second one on the right can be regarded as negligibly small. Hence, by applying Eqs. (10)–(12), the Pocklington equation changes to differential type and becomes simpler:

$$\left[\frac{\partial^2}{\partial l^2} + \gamma^2(l)\right] I(l) = -j4\pi\frac{\beta}{\psi(l) Z_0} E_z(l) = F(l) \tag{13}$$

where:

$$\psi(l) = \int_0^L g(l, l')\, \mathrm{d}l' \tag{14}$$

and:

$$\gamma^2 = \beta^2 - j4\pi\frac{\beta}{\psi(l) Z_0} Z_S(l) \tag{15}$$

The general solution of Eq. (13) cannot be sought analytically, because γ is a function of position l on the cylinder. However, by considering Eq. (2) and applying the low frequency (LF) approximation for Eq. (14) given by [10]:

$$\psi(l) = \ln\frac{L}{a} \tag{16}$$

Eq. (11) can be resolved using the parameter variation method. The solution for the current on the cylinder is given as:

$$I(l) = C_1(l)\cos(\gamma l) + C_2(l)\sin(\gamma l) \tag{17}$$

C_1 and C_2 are:

$$C_1(l) = -\int \frac{F(z)}{\gamma}\sin(\gamma l)\, dl + A \tag{18}$$

$$C_2(l) = \int \frac{F(z)}{\gamma}\cos(\gamma l) dl + B \tag{19}$$

where A and B are constants. One can reach a particular solution for the current $I(l) = I_0(l)$ by the Leibniz-Feynman method of differentiating under the integral sign in Eqs. (18)–(19) an infinite number of times, and then inserting this result into (17):

$$I_0(l) = \frac{1}{\gamma^2} \sum_{i=0}^{\infty} (-1)^i \frac{F^{(2i)}(l)}{\gamma^{2i}} \tag{20}$$

with $F^{(0)}(l) = F(l)$ (see Appendix A for the proof). Then, by using the boundary conditions for the ends of the cylinder, $I(0) = I(L) = 0$, the general solution for the current that flows through the cylinder axis is given as:

$$I(l) = I_0(l) - \frac{I_0(0)\sin[\gamma(L-l)] + I_0(L)\sin(\gamma l)}{\sin(\gamma l)} \tag{21}$$

Giving the LF approximation in Eq. (16) ($\beta\sqrt{a^2+(l-l')^2} \ll 1$) for the human of given geometry propositions, the applied frequency should be less than roughly 25 MHz. However, some of our simulations made for purposes of this paper but not depicted here indicate that model can be applied with satisfied accuracy even for higher frequencies (up to 50 MHz or more).

In its simplest form, it is possible to ignore all the terms in Eq. (21) and only keep the first one, $I_0(l) \approx F(l)/\gamma^2$. This provides an estimation of the current that still meets the boundary conditions, and it is given by:

$$I(l) \approx \frac{1}{\gamma^2}\left\{F(l) - \frac{F(0)\sin[\gamma(L-l)] + F(L)\sin(\gamma l)}{\sin(\gamma L)}\right\} \tag{22}$$

where $F(l)$ is determined by Eq. (13), and it is dependent on the distribution of the incident electric field along the cylinder. The obtained relation is a generalization of the formula for current in the case of plane wave incidence found in [10].

It is possible to calculate the body's current density once this axial current is known [30, 31]. In [32], the current density is expressed as:

$$J(\zeta, l) = \frac{I(l)}{a^2\pi}\left(\frac{\beta a}{2}\right)\frac{J_0\left(j^{-1/2}\beta\zeta\right)}{J_1\left(j^{-1/2}\beta a\right)} \tag{23}$$

where ζ ranges from 0 to a, and J_0 and J_1 are the corresponding Bessel functions. The electric field induced in the body is calculated using [36]:

$$E_{in}(\zeta, l) = \frac{J(\zeta, l)}{\sigma + j\omega\varepsilon} \tag{24}$$

where ρ is the tissue density, and σ and ε refer to the electrical properties of the human body.

$$\mathrm{SAR} = \sigma\frac{|E_{in}(\zeta, l)|^2}{\rho} \tag{25}$$

The SAR averaged per 10 g of tissue ($\mathrm{SAR}_{10\,\mathrm{g}}$) expressed by cylindrical coordinates is given by the expression [10]:

$$\mathrm{SAR}_{10\,\mathrm{g}} = \frac{1}{V_{10\,\mathrm{g}}}\iiint \mathrm{SAR}dV_c = \frac{1}{V_{10\,\mathrm{g}}}\int_0^{a_c}\int_0^{a_c}\int_0^{a_c}\mathrm{SAR}dx_c dy_c dz_c \tag{26}$$

The whole-body average SAR ($\mathrm{SAR}_{\mathrm{WB}}$) expressed by cylindrical coordinates is given by the expression [10]:

$$\mathrm{SAR}_{\mathrm{WB}} = \frac{1}{V}\iiint \mathrm{SAR}dV = \frac{1}{V}\int_0^{a}\int_0^{2\pi}\int_0^{L}\mathrm{SAR}\zeta d\zeta d\varphi dl \tag{27}$$

where V is the cylinder volume, and the surface SAR is defined as in Eq. (25).

Using Eqs. (21)–(26) and after some mathematical adjustments, Eq. (25) is given in an integral form as:

$$\mathrm{SAR}_{\mathrm{WB}} = \frac{\sigma}{\sigma^2 + (\omega\varepsilon)^2}\left(\frac{\beta}{a^2\pi}\right)^2 \frac{\displaystyle\int_0^a \zeta\left|J_0\left(j^{-1/2}\beta\zeta\right)\right|^2 d\zeta}{2\rho L\left|J_1\left(j^{-1/2}\beta a\right)\right|^2}\int_0^L |I(l)|^2 dl \tag{28}$$

3. NUMERICAL FORMULATION

The commercial software FEKO (Moments — MoM Method for Wire Antenna) was used to perform the electromagnetic modelling of the WPT system, and the surface equivalence principle (SEP) was used to apply uniformity to the dielectric body models. A perfectly electrically conducting (PEC) magnetic point source is used in the exposure scenario, along with a voltage source applied to port 1 at frequencies of 6.78 MHz and 13.56 MHz. According to the WPT standard [37], the matched transmitting antenna input power is selected to be $P_G = 5\,\mathrm{W}$. The wire segment length in FEKO is 8 mm long, and the radius of wire is 8 mm, whereas the length of edge of the triangle in human body model representation is 35 mm. The number of triangulations in the case of cylindrical equivalent model is 2350, whereas in the case of the realistic model it is 7774. As shown in Figs. 2(a) and 2(b), the magnetic dipole is positioned in front of the human model at a height of 1.2 m, which is like the worst case of [38]. The nearest distances from the body surface and the centre of the dipole are represented by the values of $d_{p1} = 30\,\mathrm{cm}$, $d_{p2} = 60\,\mathrm{cm}$, $d_{p3} = 150\,\mathrm{cm}$, and $d_{p4} = 220\,\mathrm{cm}$. The distances were chosen from the one closest to the transmitting antenna ($d_{p1} = 30\,\mathrm{cm}$) to the near-far field edge ($d_{p4} = \lambda/10$).

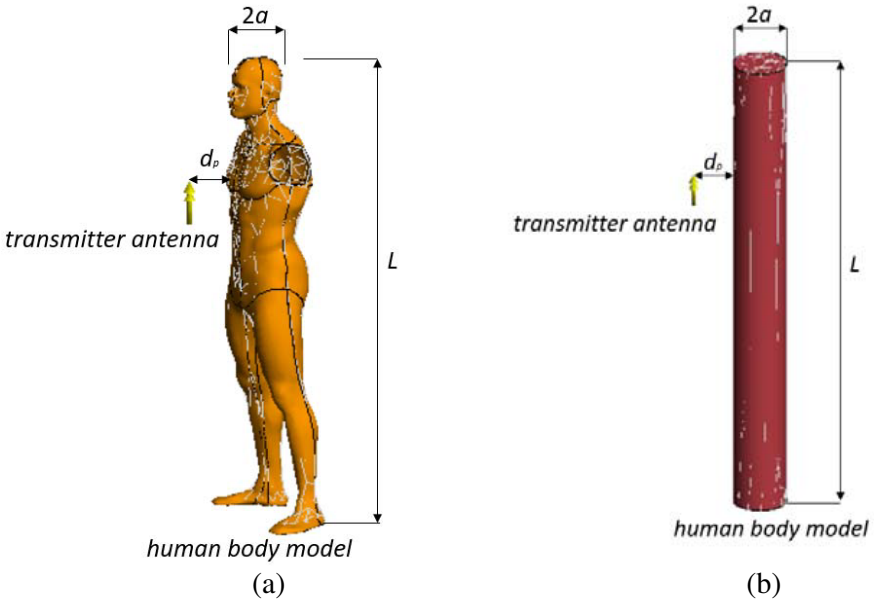

Figure 2. (a) Realistic human body model standing in free space against the transmitting short dipole, and (b) simplified equivalent cylinder human body model.

4. DISCUSSION OF THE FINDINGS

Equation (23) and Equation (24) were used to analyse the electric field E_{in} induced inside the body, and the current density J and $\mathrm{SAR}_{\mathrm{WB}}$, respectively. FEKO and Matlab were used to analyze the data numerically. At 181 points along the model of the body, the values of the incident electric field E are calculated. By multiplying the surface current by the triangle height in the direction of the cylinder axis and then by integrating from zero to 2π over the circumference of the cylinder at every position l, it is possible to determine the values of the induced current at every point of the cylindrical surface. Figures 3 to 10 show, respectively, the calculated current density J and the electric field E_{in} induced on the cylinder's surface ($\zeta = a$). At the distances under consideration, the maximum values of the induced current density and electric field are shown in Tables 1 through 4, $\mathrm{SAR}_{\mathrm{WB}}$ in Tables 5 through 6, and $\mathrm{SAR}_{10\,\mathrm{g}}$ in Tables 7 through 8, respectively, and Root Mean Square Error (RMSE) obtained in Matlab is presented Table 9 to Table 16.

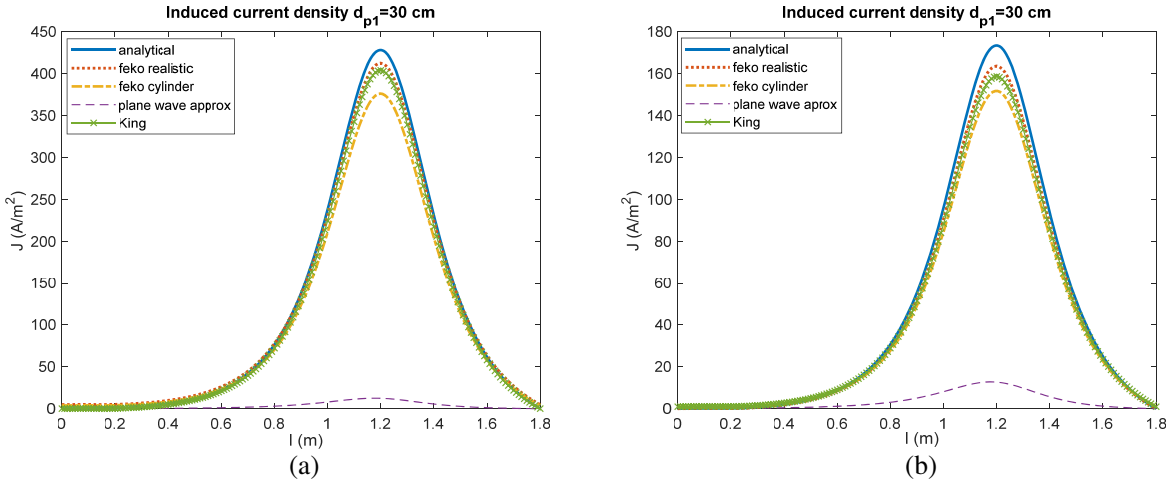

Figure 3. The distribution of the current density along the simulated human models at $d_{p1} = 30\,\text{cm}$ at (a) $f = 6.78\,\text{MHz}$, (b) $f = 13.56\,\text{MHz}$.

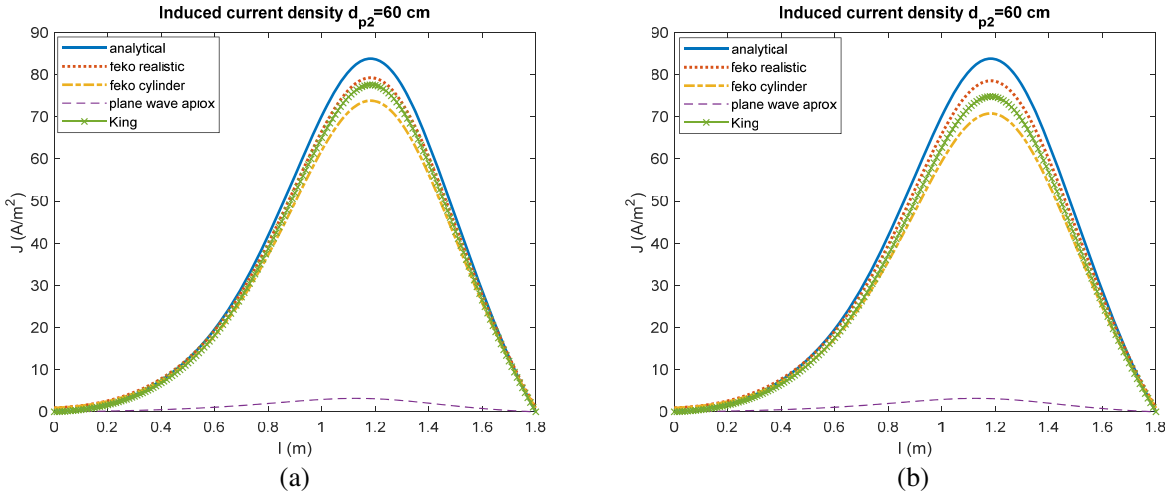

Figure 4. The distribution of the current density along the simulated human models at $d_{p2} = 60\,\text{cm}$ at (a) $f = 6.78\,\text{MHz}$, (b) $f = 13.56\,\text{MHz}$.

Table 1. Comparison among peak values of induced current density J and the fundamentals of ICNIRP [33].

	$J\ (\text{A/m}^2)$ $f = 6.78\,\text{MHz}$				*Basic ICNIRP recommendations*	
					General public	*Workers*
model	$d_{p1} = 30\,\text{cm}$	$d_{p2} = 60\,\text{cm}$	$d_{p3} = 150\,\text{cm}$	$d_{p4} = 220\,\text{cm}$		
realistic	385.4	74.09	4.952	1.322		
cylinder	351.3	69.02	4.607	1.208		
proposed analytical	427.3	83.78	5.622	1.461	**10**	**50**
King	376.5	72.35	4.806	1.285		
plane wave	12.46	3.19	0.551	0.265		

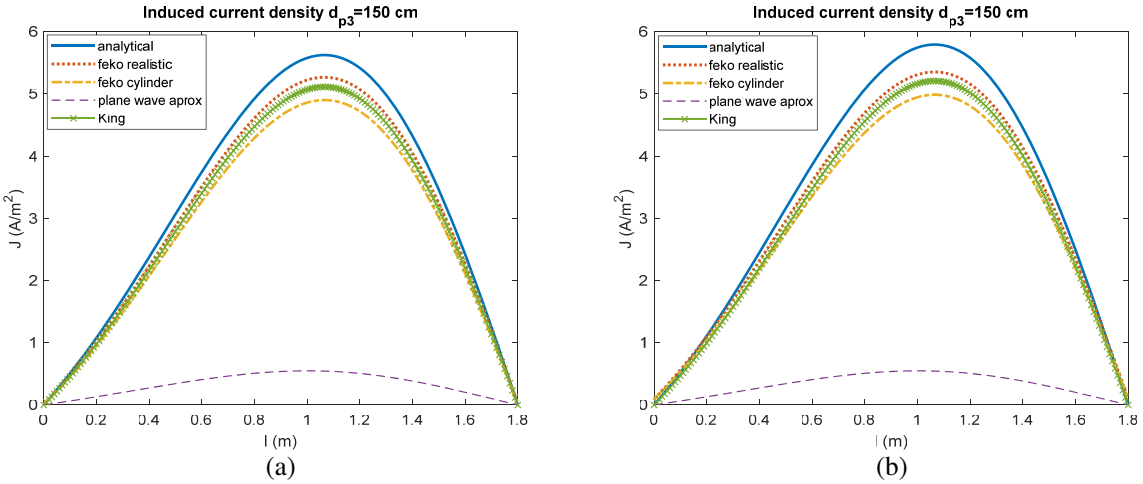

Figure 5. The distribution of the current density along the simulated human models at $d_{p3} = 150\,\text{cm}$ at (a) $f = 6.78\,\text{MHz}$, (b) $f = 13.56\,\text{MHz}$.

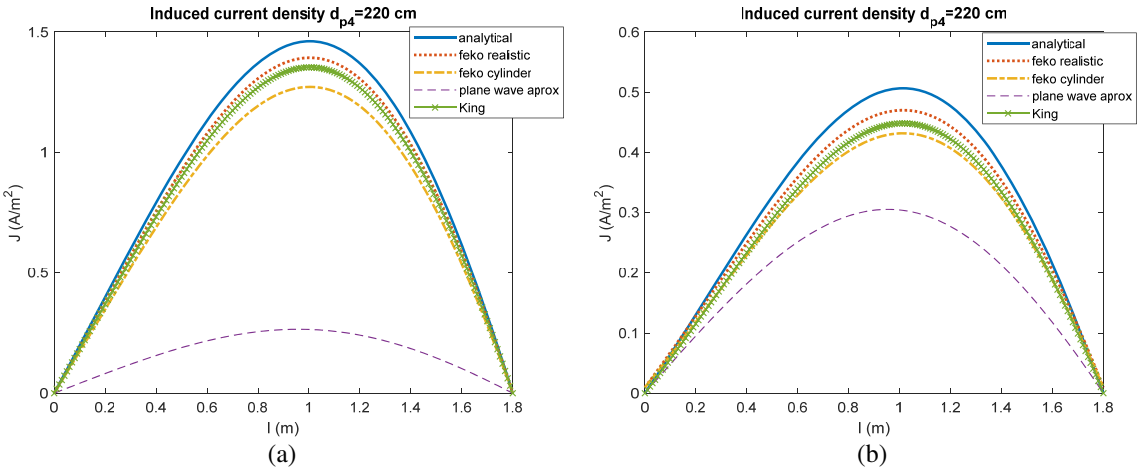

Figure 6. The distribution of the current density along the simulated human models at $d_{p4} = 220\,\text{cm}$ at (a) $f = 6.78\,\text{MHz}$, (b) $f = 13.56\,\text{MHz}$.

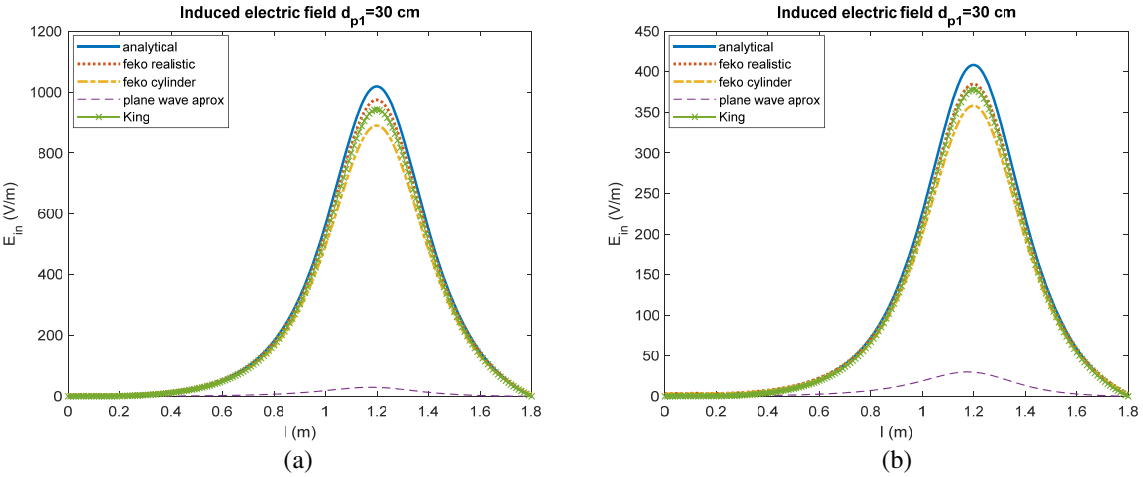

Figure 7. The distribution of the electric field induced in the simulated human models at $d_{p1} = 30\,\text{cm}$ at (a) $f = 6.78\,\text{MHz}$, (b) $f = 13.56\,\text{MHz}$.

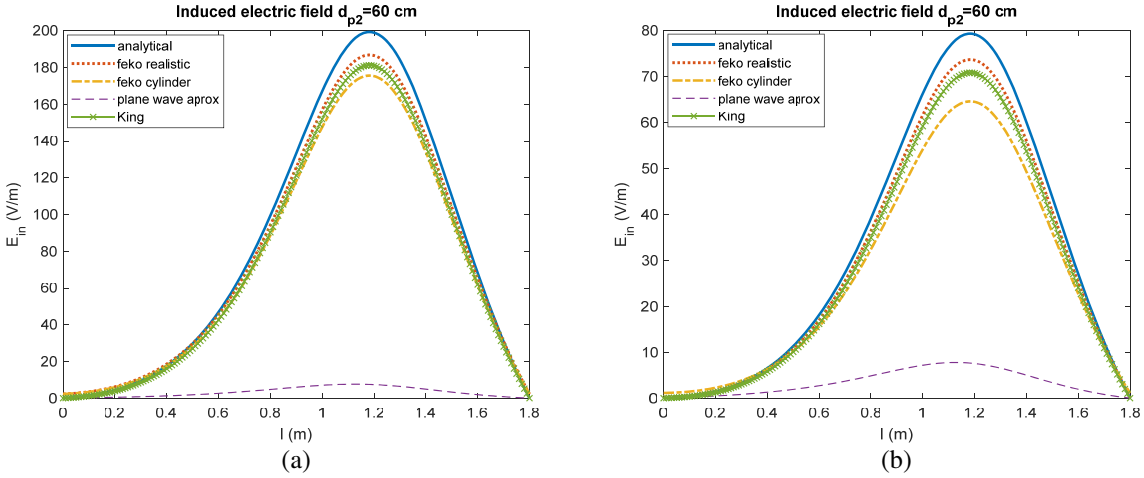

Figure 8. The distribution of the electric field induced in the simulated human models at $d_{p2} = 60\,\text{cm}$ at (a) $f = 6.78\,\text{MHz}$, (b) $f = 13.56\,\text{MHz}$.

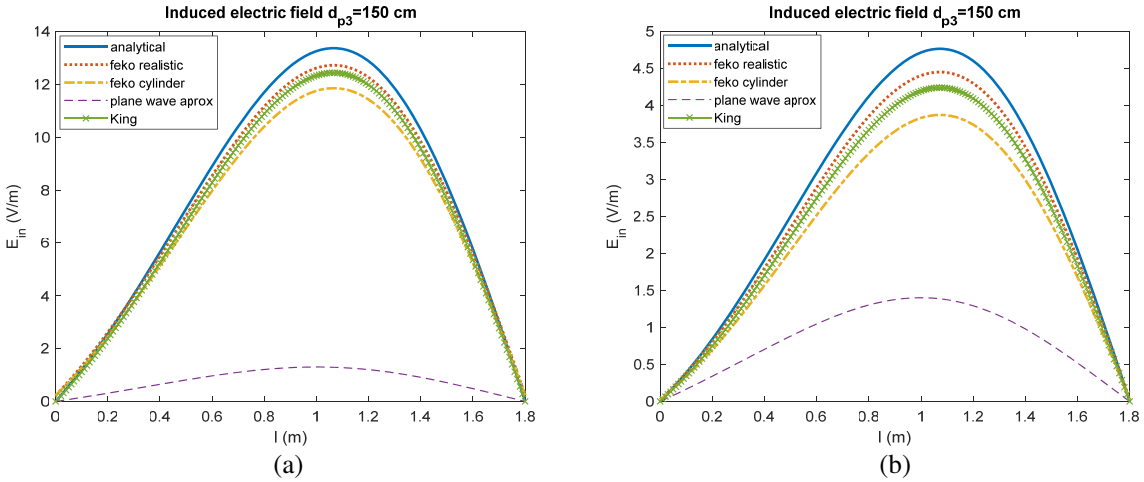

Figure 9. The distribution of the electric field induced in the simulated human models at $d_{p3} = 150\,\text{cm}$ at (a) $f = 6.78\,\text{MHz}$, (b) $f = 13.56\,\text{MHz}$.

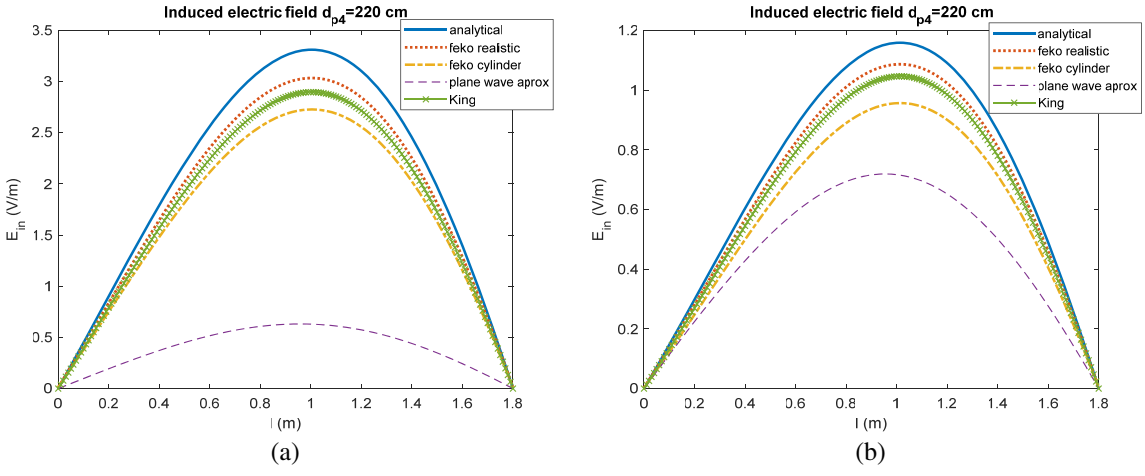

Figure 10. The distribution of the electric field induced in the simulated human models at $d_{p4} = 220\,\text{cm}$ at (a) $f = 6.78\,\text{MHz}$, (b) $f = 13.56\,\text{MHz}$.

Table 2. Comparison among peak values of induced current density J and the fundamentals of ICNIRP [33].

J (A/m^2) $f = 13.56$ MHz					*Basic ICNIRP recommendations*	
					General public	*Workers*
model	$d_{p1} = 30$ cm	$d_{p2} = 60$ cm	$d_{p3} = 150$ cm	$d_{p4} = 220$ cm		
realistic	145.5	72.57	5.038	0.432		
cylinder	134.5	66.18	4.694	0.396		
proposed analytical	173.1	83.8	5.791	0.506	**10**	**50**
King	140.7	69.89	4.897	0.411		
plane wave	12.79	3.15	0.544	0.304		

Table 3. Comparison among peak values of induced electric field inside the body E_{in} and the fundamentals of ICNIRP [33].

E_{in} (V/m) $f = 6.78$ MHz					*Basic ICNIRP recommendations*	
					General public	*Workers*
model	$d_{p1} = 30$ cm	$d_{p2} = 60$ cm	$d_{p3} = 150$ cm	$d_{p4} = 220$ cm		
realistic	909.8	174.6	11.98	2.88		
cylinder	830.1	164.2	11.16	2.59		
proposed analytical	1019.1	199.1	13.37	3.29	**78.57**	**172.86**
King	880.1	166.5	11.72	2.74		
plane wave	29.71	7.53	1.31	0.63		

Table 4. Comparison among peak values of induced electric field inside the body E_{in} and the fundamentals of ICNIRP [33].

E_{in} (V/m) $f = 13.56$ MHz					*Basic ICNIRP recommendations*	
					General public	*Workers*
model	$d_{p1} = 30$ cm	$d_{p2} = 60$ cm	$d_{p3} = 150$ cm	$d_{p4} = 220$ cm		
realistic	342.8	65.69	4.03	0.99		
cylinder	319.3	57.61	3.51	0.87		
proposed analytical	407.5	79.35	4.77	1.16	**78.57**	**172.86**
King	336.3	63.14	3.84	0.95		
plane wave	30.03	7.77	1.41	0.72		

In all scenarios, except for the ones at $d_{p1} = 30$ cm with high intensity deviation for both the general and professional populations, as well as for $d_{p2} = 60$ cm for the professional population, the maximum values of the induced electric field E_{in} and internal body current density J observed through numerical and analytical calculations are lower than the recommendations specified, as shown in Table 1 to Table 8. The SAR calculated by all considered methods is within the specified protection exposure limits. The

Table 5. Comparison among peak values of SAR_{WB} and the fundamentals of ICNIRP [33].

	$\mathbf{SAR_{WB}}$ **(W/kg)** $f = 6.78$ **MHz**				***Basic ICNIRP recommendations***	
					General public	***Workers***
model	$d_{p1} = 30$ **cm**	$d_{p2} = 60$ **cm**	$d_{p3} = 150$ **cm**	$d_{p4} = 220$ **cm**		
realistic	0.0757	0.0194	0.0021	0.0005	**0.08**	**0.4**
cylinder	0.0623	0.0181	0.0017	0.0004		
proposed analytical	0.0852	0.02422	0.0031	0.0005		
King	0.0651	0.0207	0.0024	0.0003		
plane wave	0.0053	0.0015	0.0001	0.0001		

Table 6. Comparison among peak values of $SAR_{10\,g}$ the fundamentals of ICNIRP [33].

	$\mathbf{SAR_{10\,g}}$ **(W/kg)** $f = 6.78$ **MHz**				***Basic ICNIRP recommendations***	
					General public	***Workers***
model	$d_{p1} = 30$ **cm**	$d_{p2} = 60$ **cm**	$d_{p3} = 150$ **cm**	$d_{p4} = 220$ **cm**		
realistic	1.4022	0.2252	0.0055	0.0010	**2**	**10**
cylinder	1.2649	0.1961	0.0038	0.0009		
proposed analytical	1.5504	0.27301	0.0068	0.0012		
King	1.3131	0.2057	0.0049	0.0015		
plane wave	0.1541	0.01525	0.0003	0.0005		

Table 7. Comparison among peak values of SAR_{WB} and the fundamentals of ICNIRP [33].

	$\mathbf{SAR_{WB}}$ **(W/kg)** $f = 13.56$ **MHz**				***Basic ICNIRP recommendations***	
					General public	***Workers***
model	$d_{p1} = 30$ **cm**	$d_{p2} = 60$ **cm**	$d_{p3} = 150$ **cm**	$d_{p4} = 220$ **cm**		
realistic	0.1059	0.0232	0.0024	0.0005	**0.08**	**0.4**
cylinder	0.0709	0.0199	0.0017	0.0003		
proposed analytical	0.1277	0.0314	0.0038	0.0007		
King	0.0881	0.0207	0.0022	0.0004		
plane wave	0.0055	0.0013	0.0001	0.0001		

HF heating effect measured by SAR is therefore not present for the scenarios at $f = 6.78$ MHz in contrast to the expected LF neuromuscular effect estimated by the current density and induced electric field at defined separations ($d_{p1} = 30$ cm and $d_{p2} = 60$ cm). In light of the foregoing, it can be said that for the scenarios at $f = 6.78$ MHz, the HF heating effect is not expressed in comparison to the strongly expressed LF neuromuscular effect at the defined distances ($d_{p1} = 30$ cm and $d_{p2} = 60$ cm, respectively), while the LF effect at $f = 13.56$ MHz is indicated by the transmitting antenna specific

Table 8. Comparison among peak values of $SAR_{10\,g}$ and the fundamentals of ICNIRP [33].

	$\mathbf{SAR_{10\,g}}$ **(W/kg)** $f = 13.56\,\mathbf{MHz}$				***Basic ICNIRP recommendations***	
					General public	***Workers***
model	$d_{p1} = 30\,\mathbf{cm}$	$d_{p2} = 60\,\mathbf{cm}$	$d_{p3} = 150\,\mathbf{cm}$	$d_{p4} = 220\,\mathbf{cm}$		
realistic	1.9631	0.2702	0.006	0.0011		
cylinder	1.5444	0.2071	0.004	0.0011		
proposed analytical	2.3256	0.3549	0.009	0.0014	**2**	**10**
King	1.6757	0.2157	0.005	0.0011		
plane wave	0.2695	0.0138	0.001	0.0001		

Table 9. Rootmean square error (RMSE) for current density at $f = 6.78\,\mathrm{MHz}$.

$RMSE_{CD}(\mathrm{A/m^2})f = 6.78\,\mathbf{MHz}$				
model	$d_{p1} = 30\,\mathbf{cm}$	$d_{p2} = 60\,\mathbf{cm}$	$d_{p3} = 150\,\mathbf{cm}$	$d_{p4} = 220\,\mathbf{cm}$
proposed analytical	21.5141	5.2758	0.4860	0.1328
realistic	15.7317	2.9780	0.2464	0.0849
plane wave	155.7379	38.8095	2.9323	0.7054
King	11.3760	1.9456	0.1415	0.0569

Table 10. Root mean square error (RMSE) for current density at $f = 13.56\,\mathrm{MHz}$.

$RMSE_{CD}(\mathrm{A/m^2})f = 13.56\,\mathbf{MHz}$				
model	$d_{p1} = 30\,\mathbf{cm}$	$d_{p2} = 60\,\mathbf{cm}$	$d_{p3} = 150\,\mathbf{cm}$	$d_{p4} = 220\,\mathbf{cm}$
proposed analytical	9.0399	6.9270	0.5261	0.0505
realistic	4.8881	4.2413	0.2464	0.0267
plane wave	59.3767	37.1500	3.0080	0.0886
King	2.9168	2.0837	0.1375	0.0106

distance ($d_{p1} = 30\,\mathrm{cm}$) as well as the HF effects. The radiated power must be between 0.25 W and less than 1 W in order to comply with the LF exposure guidelines established for both professionals and the general public at a distance of $d_{p1} = 30\,\mathrm{cm}$. It should be noted that the transmitting antenna frequently used in WPT has a radiation efficiency that is much lower than 100%. These results would not differentiate from the ICNIRP recommendations at any distance if a real antenna was used instead of a PEC antenna. For instance, the radiation efficiency would be 0.017% if the same transmitting antenna was constructed of copper and tuned to $f = 6.78\,\mathrm{MHz}$, with the maximum current density $J = 5.13\,\mathrm{A/m^2}$ and the maximum induced field $E_{in} = 12.19\,\mathrm{V/m}$ (tested by full-wave model in FEKO) at $d_{p1} = 30\,\mathrm{cm}$.

The proposed current approximation, given as Eq. (22), is shown to somewhat overestimate the full-wave calculation results of both real and simplified human models, whereas the cylindrical model underestimates the predictions made on the realistic one. Therefore, the results of Eq. (22) could be considered as worst-case in this scenario.

Table 11. Root mean square error (RMSE) for induced electric field at $f = 6.78\,\text{MHz}$.

$RMSE_{E_{in}}(\text{V/m})f = 6.78\,\text{MHz}$				
model	$d_{p1} = 30\,\text{cm}$	$d_{p2} = 60\,\text{cm}$	$d_{p3} = 150\,\text{cm}$	$d_{p4} = 220\,\text{cm}$
proposed analytical	53.7422	12.5485	0.9822	0.5232
realistic	35.9120	6.1404	0.5860	0.2153
plane wave	367.4453	92.3083	7.1546	1.4707
King	21.7867	2.9428	0.3638	0.1169

Table 12. Root mean square error (RMSE) for induced electric field at $f = 13.56\,\text{MHz}$.

$RMSE_{E_{in}}(\text{V/m})f = 13.56\,\text{MHz}$				
model	$d_{p1} = 30\,\text{cm}$	$d_{p2} = 60\,\text{cm}$	$d_{p3} = 150\,\text{cm}$	$d_{p4} = 220\,\text{cm}$
proposed analytical	20.7761	7.8254	0.7535	0.1808
realistic	11.4428	4.7944	0.3877	0.0907
plane wave	140.3952	31.2037	1.6474	0.1637
King	8.1299	3.2383	0.2426	0.0622

Table 13. Root mean square error (RMSE) for $\text{SAR}_{10\,\text{g}}$ at $f = 6.78\,\text{MHz}$.

$RMSE_{SAR_{10\,g}}(\text{W/kg})f = 6.78\,\text{MHz}$				
model	$d_{p1} = 30\,\text{cm}$	$d_{p2} = 60\,\text{cm}$	$d_{p3} = 150\,\text{cm}$	$d_{p4} = 220\,\text{cm}$
proposed analytical	0.0291	0.0769	0.0769	0.0096
realistic	0.0001	0.0003	0.0003	0.0006
plane wave	0.1373	0.2855	0.2855	0.0482
King	0.0001	0.0003	0.0003	0.0006

Table 14. Root mean square error (RMSE) for $\text{SAR}_{10\,\text{g}}$ at $f = 13.56\,\text{MHz}$.

$RMSE_{SAR_{10\,g}}(\text{W/kg})f = 13.56\,\text{MHz}$				
model	$d_{p1} = 30\,\text{cm}$	$d_{p2} = 60\,\text{cm}$	$d_{p3} = 150\,\text{cm}$	$d_{p4} = 220\,\text{cm}$
proposed analytical	0.0631	0.1478	0.1478	0.0086
realistic	0.0001	0.0003	0.0003	0.0006
plane wave	0.4187	0.7812	0.7812	0.1313
King	0.0001	0.0003	0.0003	0.0006

Additionally, results at the end of the string in analytical scenarios have a value of zero because of a thin wire approximation. Due to position of the transmitting antenna center, the human model's body area located at 1.2 m suffers the highest values. The peak E_{in} induced current densities J, SAR_{WB}, and $\text{SAR}_{10\,\text{g}}$ obtained in the body area of the human model at 1.2 m are also compared with the plane wave approximation defined in [10] and with King's three-term approximation [11] in Tables 1–8. As can be

Table 15. Root mean square error (RMSE) for $\mathrm{SAR_{avg}}$ at $f = 6.78\,\mathrm{MHz}$.

$RMSE_{SAR_{WB}}(\mathrm{W/kg})f = 6.78\,\mathrm{MHz}$				
model	$d_{p1} = 30\,\mathrm{cm}$	$d_{p2} = 60\,\mathrm{cm}$	$d_{p3} = 150\,\mathrm{cm}$	$d_{p4} = 220\,\mathrm{cm}$
proposed analytical	0.0134	0.0229	0.0229	0.0028
realistic	0.0001	0.0001	0.0001	0.0001
plane wave	0.0134	0.0229	0.0229	0.0028
King	0.0001	0.0001	0.0001	0.0001

Table 16. Root mean square error (RMSE) for $\mathrm{SAR_{avg}}$ at $f = 13.56\,\mathrm{MHz}$.

$RMSE_{SAR_{WB}}(\mathrm{W/kg})f = 13.56\,\mathrm{MHz}$				
model	$d_{p1} = 30\,\mathrm{cm}$	$d_{p2} = 60\,\mathrm{cm}$	$d_{p3} = 150\,\mathrm{cm}$	$d_{p4} = 220\,\mathrm{cm}$
proposed analytical	0.0350	0.0568	0.0568	0.0172
realistic	0.0002	0.0004	0.0004	0.0001
plane wave	0.0350	0.0568	0.0568	0.0172
King	0.0002	0.0004	0.0004	0.0001

noted in Figs. 4–10, the proposed approximation and King's approximation as well obey analytical and numerical results, but the plane wave approximation underestimates it more as the cylinder is closer to the transmitting antenna. It is important to note that the plane wave approximation is not good enough for the calculation in the near field; however, as we move away from the transmitting antenna and approach the far field limit, the results become closer in amplitude (for plane wave approximation and proposed analytical approximation). All these can also be seen in Tables 9 and Table 10 where the RMSE for the proposed analytical model is compared with the others (real and simplified numerical full-wave calculation in FEKO, King approximation and plane wave approximation) which is calculated for the current density results at both considered ISM frequencies. Note that the RMSE decreases with distance for all models. The plane wave approximation, however, gives significantly greater error than others until the separation between the antenna and the human model reaches the far field boundary.

5. CONCLUSION

In this work, a method for evaluating human exposure to RF fields based on a simple equivalent cylinder representation of the human body is developed numerically (full-wave calculation in FEKO), and the Pocklington Integral Differential Equations are analytically applied with excitation functions caused by the HF near-fields. $\mathrm{SAR_{WB}}$, $\mathrm{SAR_{10\,g}}$, current density, and induced electric field are estimated using both analytical and numerical methods. The analytical calculation proposed in this paper provides fast validation of the phenomenon in a form of the results that are practical in a technical sense. Furthermore, it is evident that, when using a streamlined cylindrical human body model, it is challenging to identify peak increases in narrow regions of the cross section. The maximum torso area can still be estimated using the cylindrical approximation. The simplicity and effectiveness of the methods described thus far are therefore their key characteristics.

ACKNOWLEDGMENT

The authors thank Prof. Ivanščica Mirošević, Ph.D. from the Dept. of Mathematics and Physics, for her valuable suggestions about the derived differential equation solution.

APPENDIX A.

The second derivative of the particular solution given as Eq. (20) is:

$$\begin{aligned}\frac{\partial^2 I_0(l)}{\partial l^2} &= \frac{1}{\gamma^2}\sum_{i=0}^{\infty}(-1)^i\frac{F^{(2i+2)}(l)}{\gamma^{2i}} = \sum_{i=0}^{\infty}\frac{(-1)^{-1}}{\gamma^2}(-1)^{i+1}\frac{F^{(2i+2)}(l)}{\gamma^{2i}} \\ &= -\sum_{i=0}^{\infty}(-1)^{i+1}\frac{F^{(2i+2)}(l)}{\gamma^{2i+2}} \end{aligned} \tag{A1}$$

Inserting Eq. (A1) and Eq. (20) into Eq. (13), while solving the left side of the equation, yields:

$$\begin{aligned}&-\sum_{i=0}^{\infty}(-1)^{i+1}\frac{F^{(2i+2)}(l)}{\gamma^{2i+2}} + \gamma^2\frac{1}{\gamma^2}\sum_{i=0}^{\infty}(-1)^i\frac{F^{(2i)}(l)}{\gamma^{2i}} \\ &= -\sum_{i=0}^{\infty}(-1)^{i+1}\frac{F^{(2i+2)}(l)}{\gamma^{2i+2}} + \sum_{i=0}^{\infty}(-1)^{i+1}\frac{F^{(2i+2)}(l)}{\gamma^{2i+2}} + F(l) = F(l)\end{aligned} \tag{A2}$$

Because the left side equals the right side, the proof is complete.

APPENDIX B.

The approach used by King to acquire better near fields is to first find an improved solution for the present $I(l)$ and then utilize it to compute the field $E_l(l)$ [11, 15]:

$$\begin{aligned}I(l) &= A_1\left[\sin\left(\beta\left|l-\frac{L}{2}\right|\right) - \sin\left(\beta\frac{L}{2}\right)\right] + A_2\left\{\cos\left[\beta\left(l-\frac{L}{2}\right)\right] - \cos\left(\beta\frac{L}{2}\right)\right\} \\ &\quad + A_3\left\{\cos\left[\frac{\beta\left(l-\frac{L}{2}\right)}{2}\right] - \cos\left(\frac{\beta L}{4}\right)\right\}\end{aligned} \tag{B1}$$

and fix the coefficients A_1, A_2, A_3 by fitting this expression to the numerical solution. The required quantities appearing in Eq. (B1) are calculated as follows [15]:

$$\frac{\partial^2 I(l')}{\partial l^2} + \beta^2 I(l') = -\beta^2 A_1\sin\beta\frac{L}{2} - \beta^2 A_2\cos\beta\frac{L}{2} - \beta^2 A_3\left[\cos\left(\frac{\beta L}{4}\right) - \frac{3}{4}\cos\left(\frac{\beta l'}{2}\right)\right] \tag{B2}$$

$$I'(0+) = -I'(0-) = \beta A_1 \tag{B3}$$

$$\frac{\partial I}{\partial l}\left(\frac{L}{2}\right) = -\frac{\partial I}{\partial l}\left(-\frac{L}{2}\right) = \beta A_1\cos\beta\frac{L}{2} - \beta A_2\sin\beta\frac{L}{2} - \frac{1}{2}\beta A_3\sin\left(\frac{\beta L}{4}\right) \tag{B4}$$

REFERENCES

1. International Commission on Non-Ionizing Radiation Protection (ICNIRP), "Guidelines for limiting exposure to electromagnetic fields (100 kHz to 300 GHz)," *Health Physics*, Vol. 118, 483–524, 2020.
2. Reilly, J. P., *Applied Bioelectricity: From Electrical Stimulation to Electro Pathology*, Springer Science & Business Media, New York, NY, USA, 2012.
3. WHO — World Health Organization, "Electromagnetic fields (300 Hz–300 GHz)," Environmental Health Criteria, Vol. 137, World Health Organization, Geneva, Switzerland, 1993.
4. Fish, R. M. and L. A. Geddes, "Conduction of electrical current to and through the human body: A review," *ePlasty: Open Access Journal of Plastic Surgery*, Vol. 9, 407–421, 2009.
5. WHO — World Health Organization, "Extremely low frequency fields," Environmental Health Criteria, Vol. 238, World Health Organization, Geneva, Switzerland, 2007.
6. Gryz, K. and J. Karpowicz, "Principles for electromagnetic hazards assessment related to induced and contact currents," *Podstawy I Metod, Oceny Srodowiska*, Vol. 4, 137–171, 2008.

7. Kavet, R., R. A. Tell, and R. G. Olsen, "Radiofrequency contact currents: Sensory responses and dosimetry," *Radiat. Prot. Dosim.*, Vol. 162, 268–279, 2014.
8. Scientific Committee on Emerging and Newly Identified Health Risks (SCENIHR), "Potential health effects of exposure to electromagnetic fields (EMF)," European Commission, 1–288, Brussels, Belgium, 2015.
9. Tell, R. A. and C. A. Tell, "Perspectives on setting limits for RF contact currents: A commentary," *Biomed. Eng.*, Vol. 17, 2018.
10. Poljak, D., "Human exposure to non-ionizingradiation," Kigen, Zagreb, 2006.
11. http://eceweb1.rutgers.edu/∼orfanidi/ewa/ch25.pdf, Dec. 1, 2022.
12. Gandhi, O. P. and J. Y. Chen, "Numerical dosimetry at power line frequencies using anatomically based models," *Bioelectromagnetics Suppl.*, Vol. 1, 43–60, 1992.
13. Chiba, A., K. Isaka, and Y. Onogi, "Analysis of current densities induced inside human model by the two-steps process method combining the surface integral equation and the finite element method," *Electronics and Communication in Japan*, Part 2, Vol. 79, No. 4, 1994.
14. Gonzales, C., A. Peratta, and D. Poljak, "Boundary element modelling of the realistic human body exposed to extremely low frequency (ELF) electric fields: Computational and geometrical aspects," *IEEE Trans. Electromagn. Compat.*, Vol. 49, No. 1, 153–162, 2007.
15. Gonzalez, C., A. Peratta, and D. Poljak, "Induced currents in the human body resulting from the proximity to surfaces at fixed potentials," *Proceedings SoftCOM 2007*, 139–143, University of Split, FESB, 2007.
16. Gonzalez, C., A. Peratta, and D. Poljak, "Human body exposure to fixed potential surfaces in power substations," *Modelling in Medicine and Biology VII*, 243–252, WIT Press, Brebbia, Carlos A. (ur.), Southampton, 2007.
17. Čavka, D., D. Poljak, A. Peratta, and C. Brebbia, "Boundary element model of the human heas exposed to electrostatic field generated by Video Display Units," *Boundary Elements and Other Mesh Reduction Method XXX*, L. Škerget, C. A. Brebbia, 115–124, WIT Press, Southampton, 2008.
18. Gonzalez, C., A. Peratta, and D. Poljak, "Pregnant women exposes to extremely low frequency electromagnetic fields," *Proceedings of 2008 International Conference on Software, Telecommunications and Computer Networks*, University of Split, FESB, 2008.
19. Gonzalez, C., A. Peratta, and D. Poljak, "Electromagnetic modeling of fetus and pregnant women exposed to extremely low frequency electromagnetic fields," *Boundary Elements and Other Mesh Reduction Methods XXX/Southampton*, 85–94, WIT Press, 2008.
20. Gandhi, O. P., "Some numerical methods for dosimetry: Extremely low frequencies to microwave frequencies," *Radio Sci.*, Vol. 30, No. 1, 161–177, Jan.–Feb. 1995.
21. Gandhi, O. P., Y. Gu, Y. J. Y. Chen, and H. I. Bassen, "Specific absorption rates and induced current distributions in anatomically based model for plane wave exposures," *Health Physics*, Vol. 63, No. 3, 281–290, Spet. 1992.
22. Dawson, T. W., K. Caputa, and M. A. Stuchly, "High-resolution organ dosimetry for human exposure to low frequency electric fields," *IEEE Trans. Power Delivery*, Vol. 13, No. 2, 366–373, Apr. 1998.
23. Laakso, I., T. Shimamoto, A. Hirata, and M. Feliziani, "Applicability of quasistatic approximation for exposure assessment of wireless power transfer," *2014 International Symposium on Electromagnetic Compatibility*, Tokyo, 2014.
24. Hirata, A., S. Tsuchida, and I. Laakso, "Variability of SAR in different human models due to wireless power transfer with magnetic resonance," *2013 International Symposium on Electromagnetic Compatibility*, 2013.
25. Hirata, A., T. Sunohara, I. Laakso, and T. Onishi, "SAR in a simplified human model due to wireless power transfer with induction coupling," *2013 7th European Conference on Antennas and Propagation (EuCAP)*, 2013.

26. Christ, A., M. Douglas, J. Nadakuduti, and N. Kuster, "Assessing human exposure to electromagnetic fields from wireless power transmission systems," *Proceedings of the IEEE*, Vol. 101, No. 6, 1482–1493, 2013.
27. Koohestani, M., M. Ettorre, and M. Zhadobov, "Wireless power transfer: Are children more exposed than adults?" *2017 11th European Conference on Antennas and Propagation (EUCAP)*, 2017.
28. Laakso, T. I., A. Hirata, and T. Onishi, "Induced field and SAR in human body model due to wireless powertransfer system with induction coupling," *2014 International Symposium on Electromagnetic Compatibility*, Tokyo, 2014.
29. Yuan, Q., Y. Chen, L. Li, and K. Sawaya, "Numerical analysis on transmission efficiency of evanescent resonant coupling wireless power transfer system," *IEEE Trans. Antennas Propag.*, Vol. 58, No. 5, 1751–1758, May 2010.
30. Christ, A., M. G. Douglas, J. M. Roman, E. B. Cooper, A. P. Sample, B. H. Waters, J. R. Smith, and N. Kuster, "Evaluation of wireless resonant power transfer systems with human electromagnetic exposure limits," *IEEE Trans. Electromagn. Compat.*, Vol. 55, No. 2, 265–274, Apr. 2013.
31. Chen, X. L., A. E. Umenei, D. W. Baarman, N. Chavannes, V. De Santis, J. R. Mosig, and N. Kuster, "Human exposure to close-range resonant wireless power transfer systems as a function of design parameters," *IEEE Trans. Electromagn. Compat.*, Vol. 56, No. 5, 1027–1034, Oct. 2014.
32. IEEE Standard for Safety Levels with Respect to Human Exposure to Radio Frequency Electromagnetic Fields, 3 kHz to 300 GHz, C95, IEEE, New York, 2005.
33. ICNIRP, "Guidelines for limiting exposure to time-varying electric magnetic and electromagnetic fields (up to 300 GHz)," *Health Physics*, Vol. 74, 494–522, 1998.
34. Rasic, P., Z. Blaževic, D. Poljak, and M. Skiljo, "A simplified analytical model for human exposure to electromagnetic radiation of HF wireless power transmitter," *Splitech 2022*, 2022.
35. IT'IS Database, http://www.itis.ethz.ch/virtual-population/tissue-properties/database/dielectric-properties.
36. King, R. W. P., "Electric current and electric field induced in the human body when exposed to an incident electric field near the resonant frequency," *IEEE Trans. Microwave Theory and Tech.*, Vol. 48, No. 9, 1537–1543, Sept. 2000.
37. Tseng, R., B. von Novak, S. Shevde, and K. A. Grajski, "Introduction to the alliance for wireless power loosely-coupled wireless power transfer system specification version 1.0," *Proceedings of Wireless Power Transfer (WPT)*, 79–83, Perugia, Italy, May 15–16, 2013.
38. Lee, J. and S. Nam, "Fundamental aspects of near-field coupling small antennas for wireless power transfer," *IEEE Trans. Antennas Propag.*, Vol. 58, No. 12, 3442–3449, 2010.